AIMS Energy, 14(1): 115–139.
DOI: 10.3934/energy.2026005
Received: 20 June 2025
Revised: 26 November 2025
Accepted: 03 December 2025
Published: 16 January 2026

https://www.aimspress.com/journal/energy

Research article

Analysis of the dynamic performance and energy efficiency of a three-wheel electric vehicle under standard drive cycles

M M Mostafa Almadani[1,*], Omowunmi Mary Longe[1], Lanre Olatomiwa[1,2] and Tobiloba Somefun[1]

[1] Department of Electrical and Electronic Engineering Science, University of Johannesburg, Johannesburg 2006, South Africa
[2] Department of Electrical and Electronics Engineering, Federal University of Technology, Minna, Nigeria

* **Correspondence:** Email: 222241561@student.uj.ac.za; Tel: +27820872862.

Abstract: Electric three-wheelers are increasingly adopted in developing countries as sustainable alternatives to internal combustion engine-based transport, yet their design and optimization require accurate modelling tools for improved adoption. This study develops a comprehensive MATLAB/Simulink model for evaluating the dynamic performance and energy efficiency of a three-wheel electric vehicle under standard driving cycle conditions. The model integrates a 3 kW brushless DC (BLDC) motor, a 48 V 100 Ah lithium-ion battery (NMC), and an H-bridge inverter with regenerative braking. The motor electrical parameters, battery internal resistance, C-rate, and inverter switching characteristics were incorporated to ensure reproducibility. A proportional-integral (PI) controller is employed to emulate driver torque demand. Vehicle performance is assessed using four standard drive cycles, such as the federal test procedure (FTP-75), the new European driving cycle (NEDC), the worldwide harmonized light vehicles test procedure (WLTP Class 3), and the urban dynamometer driving schedule (UDDS). Results show that WLTP Class 3 provides the most realistic representation of energy consumption for urban three-wheelers owing to its wider speed range, more dynamic acceleration patterns, and mixed urban–suburban characteristics. In comparison, FTP-75 and UDDS emphasise low-speed stop-and-go operation, while NEDC reflects smoother peri-urban driving. A mass-based analysis further demonstrates a strong positive correlation between vehicle weight and energy consumption, offering insight for chassis design, payload limits, and operational planning. The proposed framework provides a scalable, cost-effective tool that supports EV retrofit programs and guides manufacturers in optimising motor sizing, controller tuning, and battery capacity for three-wheel electric mobility in developing regions.

Keywords: three-wheel electric vehicle; MATLAB/Simulink; drive cycle; H-bridge; State-of-Charge (SoC); longitudinal driver

1. Introduction

Climate change, global warming, and rising fuel costs are significant challenges confronting humanity today [1]. Recent research has emphasised the critical role of exploring renewable energy sources as a sustainable solution to combat climate change, mitigate global warming, and reduce dependence on fossil fuels [1]. Fluctuating fuel prices are placing growing financial pressure on consumers. In response, vehicle manufacturers are increasingly adopting cleaner technologies to reduce emissions and improve fuel efficiency. Pollution reduction is essential not only for environmental sustainability but also for managing consumer costs. Rising carbon dioxide (CO_2) levels and the visible impacts of global warming highlight the urgent need for energy-efficient, low-emission vehicles, as supported by recent research [2]. Air pollution has recently become a serious problem in metropolitan cities. One liter of gasoline produces approximately 2.3 kg of CO_2. This means that an average vehicle, which consumes about 2000 L of gasoline annually, releases nearly 4600 kg of CO_2 into the atmosphere every year [3]. As a result, battery-powered electric vehicles (EVs) are emerging as a promising solution to combat both environmental pollution and the energy crisis. The automotive industry is shifting from internal combustion engine (ICE) to EVs to reduce fossil fuel emissions. Globally, EVs are being actively promoted as a cleaner and more sustainable transportation option [1,4].

ICE three-wheelers have played a crucial role in providing affordable and efficient transportation in many parts of the world, especially in Asia, Africa, and Latin America. Commonly used as auto-rickshaws or small cargo carriers, these vehicles are typically powered by small petrol, diesel, or compressed natural gas (CNG) engines. Their lightweight design, low maintenance cost, and ability to navigate congested urban areas have made them a popular choice for last-mile connectivity and short-distance travel. However, ICE three-wheelers also pose significant environmental challenges. Older models often lack modern emission control technologies, resulting in the release of high levels of pollutants, such as carbon monoxide (CO), hydrocarbons (HC), and nitrogen oxides (NOx). Additionally, the noise generated by their engines contributes to urban noise pollution, affecting public health and quality of life [5].

The motivation for converting to EVs primarily stems from the need to address environmental and economic challenges associated with traditional gasoline- and diesel-powered vehicles. EVs produce zero tailpipe emissions, significantly reducing air pollution and contributing to the fight against climate change [6]. Additionally, rising fuel prices have made electricity a more cost-effective and stable energy source. Electric motors are also more energy-efficient and require less maintenance due to fewer moving parts, which lowers operating costs over time. Advances in battery technology have further improved the driving range and charging convenience of EVs, making them a practical alternative. Governments worldwide are promoting the adoption of EVs through incentives and policies aimed at reducing carbon footprints. Furthermore, EVs offer quieter operation, reducing noise pollution in urban areas. Together, these factors motivate the shift toward electric mobility as a sustainable, efficient, and economically viable solution for the future of transportation [6]. Figure 1, drawn using SolidWorks [7], shows a typical three-wheel EV (commonly referred to as a tuktuk or auto-rickshaw), which is the focus of this study. These vehicles are widely used for urban passenger

and cargo transport in developing countries due to their affordability and manoeuvrability in congested traffic.

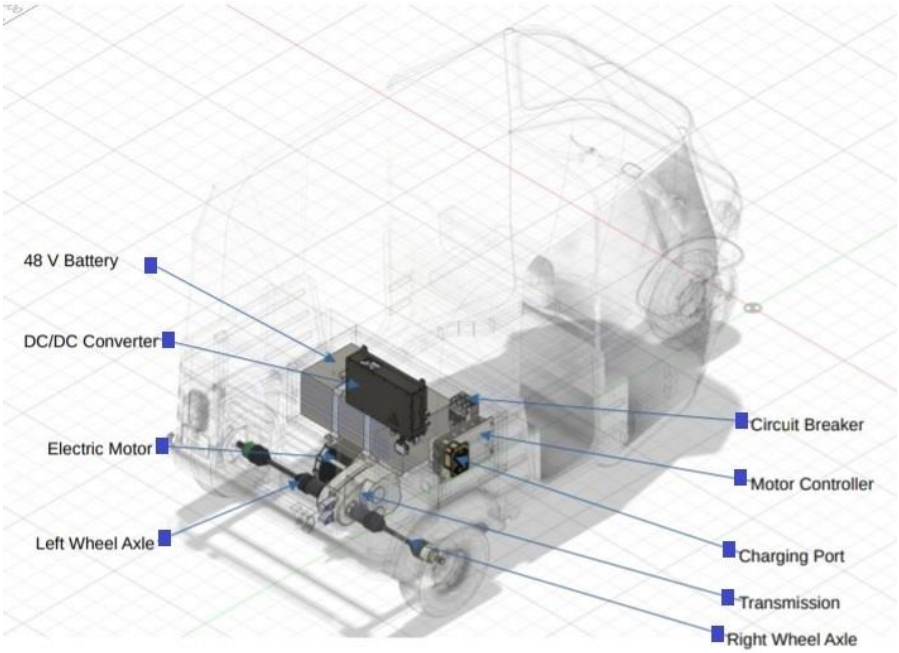

Figure 1. Typical three-wheel EV (tuktuk) used in urban transportation.

Existing EV modelling studies often oversimplify system dynamics, lack integration of key components, and inadequately reflect real-world driving conditions. Most focus on four-wheeled vehicles, with limited attention to the unique dynamics of three-wheeled EVs [8]. While Hossain et al. [8] explored prospects and challenges of affordable three-wheel EVs in Bangladesh from a policy and sustainability perspective, the present study complements this by focusing on the technical modelling and energy performance analysis. This research aims to develop a comprehensive MATLAB/Simulink simulation model of a three-wheeled EV, integrating key subsystems, such as the vehicle body, DC motor, H-bridge, and control systems. Objectives include modelling the vehicle's unique characteristics, unifying subsystem integration, evaluating performance using standard drive cycles, and analyzing system behavior for future optimization and real-world application. Despite extensive work on four-wheel EVs, there remains limited literature addressing the system-level modelling of three-wheel EVs using standardized global drive cycles. Most existing studies focused on simplified vehicle or motor-level analyses [1]. This study fills that gap by adopting the worldwide harmonized light vehicles test procedure (WLTP Class 3) drive cycle, a modern test procedure that realistically captures speed variability, acceleration intensity, and load transitions into the modelling of a typical urban tuktuk operation. The main objectives of this research are to develop a comprehensive simulation framework for a three-wheel EV integrating all major subsystems, evaluate its dynamic performance and energy efficiency under standardized drive cycles, and analyze mass-dependent energy consumption trends for design optimization.

The rest of the paper is organised as follows: Section 2 comprehensively reviews the existing literature, highlighting current modelling approaches and their limitations. Section 3 describes the

detailed methodology used to develop the integrated simulation model, including subsystem modelling and control strategy implementation. Section 4 presents the simulation results, including performance analysis under various operating conditions and validation against benchmark data. Finally, Section 5 concludes the paper by summarising the main findings, outlining the contributions, and suggesting directions for future research.

2. Literature review

EV conversion has become a practical option for individuals and organisations aiming to switch to EVs without bearing the high costs of buying a new one. The lower expense of converting an ICE vehicle to electric, compared to purchasing a brand-new EV, is a key factor driving the growing interest in EV conversions, especially in developing countries.

Several studies have explored the practicality of EV conversions, highlighting both their benefits and challenges. Vrazic et al. [9], conducted a detailed case study showing that, despite technical difficulties in integrating key components like motors and batteries, conversions can meet modern safety and performance standards when done properly. The CEPIUM project in Portugal further demonstrated that such conversions can comply with local regulations, supporting the idea that EV conversion is a viable and cost-effective alternative to purchasing new EVs [9]. Qiao et al. [10] examined the recycling of key EV components, particularly lithium-ion batteries, and emphasised its environmental benefits. Their study found that recycling reduces waste and lowers the carbon footprint of EV conversions. This indicates that integrating effective recycling practices with EV conversions can significantly improve the overall environmental sustainability of the EV sector. EV conversions, particularly for three-wheelers, have become a growing focus of research and development due to the need for cleaner, more affordable urban transportation. Several past studies have explored the feasibility, design, and performance of converting conventional ICE three-wheelers into EVs.

Many studies focus on the mechanical and electrical redesign required for EV conversions. These include replacing the ICE with an electric motor, integrating a battery pack, designing control systems, and modifying the drivetrain and chassis. For example, Gautam et al. [11] conducted a feasibility study on converting auto-rickshaws to electric power, considering motor selection, battery sizing, and drivetrain modifications. Suryavanshi et al. [12] demonstrated the conversion process of a three-wheeler to electric using BLDC motors and lithium-ion batteries, achieving notable improvements in efficiency and emission reduction.

Several studies highlight the environmental and economic benefits of converting ICE vehicles to electric power, particularly in densely populated regions where three-wheelers are commonly used for urban transport. Researchers, such as Kulkarni et al. [13], have explored the feasibility of retrofitting ICE-based auto-rickshaws with electric drivetrains, emphasizing reductions in operating costs and emissions. Their work demonstrated the importance of component selection, particularly the battery and motor in achieving acceptable range and performance. Similarly, Pandit et al. [14] modelled EV powertrains using MATLAB/Simulink and found that simulation-based design significantly improves system integration and tuning of controllers for motor efficiency and battery management.

In the context of vehicle dynamics, Gebisa et al. [15] developed a Simulink-based model for lightweight EVs, incorporating drive cycles and terrain profiles to evaluate real-world performance. Their findings stressed the importance of accurate modelling of torque-speed characteristics and regenerative braking for urban mobility solutions. Furthermore, studies focusing on three-wheeled EVs

have addressed their unique stability, load distribution, and drivetrain configuration issues. For instance, Tiwary et al. [16] emphasized optimizing energy consumption for three-wheelers by simulating various drive cycles like the new European driving cycle (NEDC) and the federal test procedure (FTP-75). Their work also integrated SOC-based battery models to reflect realistic usage conditions.

Overall, the literature supports the use of MATLAB/Simulink as a reliable platform for modelling, simulation, and performance validation of EV conversions. However, there remains a gap in simulation studies focused specifically on three-wheel vehicle conversions in developing nations, where these vehicles are most prevalent. This study aims to fill that gap by providing a comprehensive simulation framework for evaluating the performance of a converted electric three-wheeler under real-world driving conditions.

3. Methodology

The methodology for this study involves the modelling, and simulation of a three-wheel EV using MATLAB/Simulink. The process begins with defining the vehicle's performance requirements, including speed, range, and load capacity. Based on these parameters, key components, such as the electric motor, battery pack, controller, and vehicle body, are selected and modelled. A DC motor is used to drive the vehicle, with a battery providing the necessary power. The motor controller, along with an H-bridge inverter, is implemented to regulate motor operation through PWM signals. The vehicle body is modelled to account for dynamics, such as mass, aerodynamic drag, and rolling resistance. All components are integrated into a single Simulink environment to simulate the overall EV system. Four different standard driving cycles are applied to test vehicle performance under real-world conditions.

3.1. System design

The vehicle consists of several main components, including the vehicle body, the DC motor, the power converter, the battery, the drive controller, and the drive cycle. Figure 2 presents the block diagram, which illustrates the basic architecture of the electric three-wheel vehicle. The choice of the above components is justified by the operational profile of three-wheelers (tuktuks) used in urban transport [17,18]. All component selections were guided by practical tuktuk specifications and literature-based benchmarks to ensure representativeness and reproducibility. The chosen 3 kW motor, 48 V-100 Ah NMC battery, and 670 kg curb weight align with commercially available electric tuktuk configurations [18]. Input parameters were validated against published design data [17,18] to maintain a realistic model. The H-bridge inverter was sized to support the required peak motor current while ensuring efficiency during regenerative braking. Together, these specifications achieve the vehicle's design targets: top speed ~60 km/h, typical range ~50 km, and payload ~200 kg. Furthermore, the simulation framework allows direct parameter adjustment for verification and replication by other researchers.

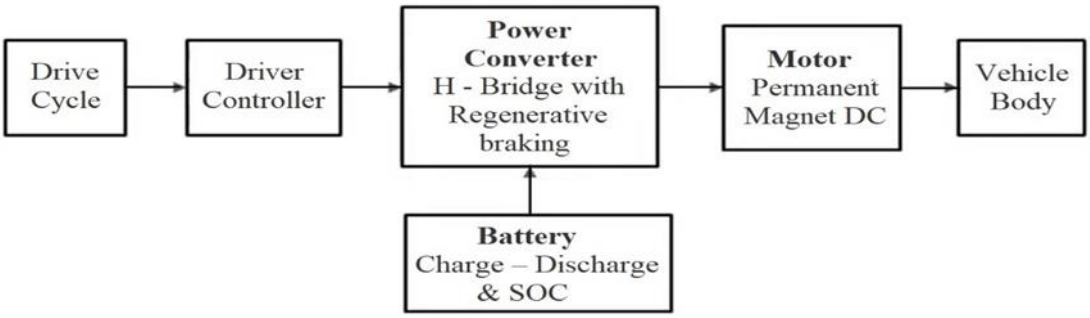

Figure 2. Block diagram of the proposed electric tuktuk model.

3.1.1. Drive cycle

Drive cycle is a standardized series of driving conditions used to evaluate the energy consumption, performance, and efficiency of EVs. It serves as the input to the vehicle. It simulates real-world driving scenarios such as acceleration, deceleration, speeds, cruising, and idle times. These cycles are essential for determining key metrics like range, energy efficiency, and emissions under typical driving conditions. More than 256 driving cycles exist around the world [17]. Some well-known drive cycles for EVs are the WLTP, the NEDC, the FTP-75, urban dynamometer driving schedule (UDDS), the world harmonized vehicle cycle (WHVC), Japan 10-15 mode, New York City cycle (NYCC), etc. Four major drive cycles deploy in this study are presented in Table 1 [18,19].

Table 1. Summary of FTP-75, NEDC, WLTP Class 3, and UDDS drive cycles.

Drive cycle	Description	Region	Simulation period
FTP-75	Designed by the U.S. EPA, this cycle simulates typical city driving, including frequent stops, idling, and low to moderate acceleration. It consists of cold start, transient, and hot start phases.	United States	2474 seconds
NEDC	Developed to assess fuel economy and emissions under urban and extra-urban conditions. Considered outdated due to unrealistic driving behavior (gentle accelerations, long idle periods).	Europe	1180 seconds
WLTP Class 3	A modern test cycle that replaces NEDC in many regions. It simulates realistic driving behavior with a combination of urban, suburban, and highway segments, reflecting modern traffic conditions and vehicle performance.	Global/International	1800 seconds
UDDS	Represents stop-and-go traffic in urban environments, mainly for light-duty vehicles. It includes low speeds and gradual accelerations and is used for emission and energy consumption testing.	United States	1369 seconds

Although three-wheel EVs are predominantly used in Asian and African cities, the selection of standardized global drive cycles is essential for producing reproducible and comparable performance

assessments. Each of the chosen cycles captures key operational characteristics that are directly relevant to the real-world behavior of commercial three-wheelers. The FTP-75 represents dense urban driving with frequent stops, short acceleration bursts, and low-to-medium operating speeds—conditions commonly experienced by three-wheel taxis during city center operations, passenger loading, and congested traffic flow. UDDS similarly reflects stop-and-go driving but includes short cruising periods and softer accelerations, making it suitable for modelling three-wheelers operating on feeder roads and inner-urban corridors. NEDC incorporates smoother acceleration patterns and moderate average speeds, resembling peri-urban trips and semi-structured routes undertaken by three-wheel goods and passenger carriers between markets, schools, and residential clusters. WLTP Class 3, although designed for light-vehicle certification, provides a more realistic and dynamically rich profile with mixed low, medium, and high-speed phases. Its greater speed variability, longer accelerations, and transient dynamics closely mirror the driving behavior of three-wheelers in large Asian and African cities, where these vehicles frequently transition between urban congestion, arterial middle-speed segments, and short open-road stretches.

Collectively, these cycles enable a comprehensive evaluation of three-wheeler performance across operating scenarios typical of developing-country transport systems. While all of them have some features that may support electric 3-wheel vehicles, the optimal drive cycle would be appreciated. Therefore, the detailed simulation and analysis of these driving cycles with regard to their application in an electric 3-wheel vehicle are discussed in Section 4 of this paper.

3.1.2. Driver controller

The Driver Controller simulates the behavior of a human driver by comparing the reference speed from the drive cycle with the actual vehicle speed. A proportional-integral (PI) controller was implemented to minimize the speed error and generate a throttle or braking signal accordingly. The output modulates the H-bridge via a PWM logic to adjust motor torque in real-time.

3.1.3. H-bridge inverter

An H-bridge inverter topology was implemented to control the bidirectional power flow between the battery and motor. The H-bridge inverter consists of four IGBT switches rated at 600 V, 50 A, with freewheeling diodes for bidirectional current flow. It operates under sinusoidal PWM at 10 kHz, providing torque control in both motoring and regenerative braking modes. The inverter is sized to match the motor's continuous current (50–70 A) and voltage rating (48 V nominal). Its selection ensures efficient operation while keeping switching and conduction losses minimal for a light electric three-wheeler. Regenerative braking is achieved by routing negative torque current back into the battery, raising SOC during deceleration events.

$$E_b = K_e \cdot \omega \tag{1}$$

$$I_{regen} = \frac{E_b - V_{bat}}{R_{system}} \tag{2}$$

$$T = -K_t \cdot I_{regen} \tag{3}$$

where E_b is the back electromotive force (V), K_e is the motor back EMF constant (Vs/rad or V/rpm), ω is the angular speed of the motor (rad/s), I_{regen} is the current flowing back into the battery during braking (A), V_{bat} is the battery voltage (V), R_{system} is the total series resistance (Ω), T is the electromagnetic torque (Nm), and K_t is the motor torque constant (Nm/A).

3.1.4. Battery system

The battery system consists of a 48 V, 100 Ah lithium-ion pack based on NMC (Nickel Manganese Cobalt) chemistry, with an energy capacity of 4.8 kWh. The pack comprises 13 series-connected cells (3.7 V nominal per cell, 100 Ah), with an internal resistance of 50 mΩ. The maximum continuous discharge rate is 2C (200 A), which is sufficient to meet the motor's peak current demand of ~70 A. The selection of this pack balances vehicle range (~50 km under typical urban driving), weight (~35 kg), and cost considerations. NMC chemistry was chosen for its relatively high energy density, cycle life of >1000 cycles at 80% DOD, and moderate thermal stability, making it suitable for low-cost electric tuktuk applications. The internal resistance model captures voltage sag during high current acceleration and regenerative charging. The battery supplies energy during motoring and receives energy during braking. SOC is estimated using the equation:

$$SOC(t) = SOC_0 + \frac{1}{C_{nominal}} \int_0^t I(t')\, dt' \tag{4}$$

where $SOC(t)$ is the state of charge at time t, SOC_0 is the initial state of charge at $t = 0$, $C_{nominal}$ is the nominal capacity of the battery, and $I(t')$ is the current at time t'.

The Simscape battery block tracks SOC and provides real-time feedback on the energy status, enabling analysis of range, energy efficiency, and regeneration effectiveness. The current SOC model is based on ideal Coulomb counting, which does not account for temperature effects, battery aging, or voltage sag during high current loads. These factors will be incorporated in future work to improve accuracy.

3.1.5. Motor and power control system

A brushless DC (BLDC) motor rated at 3 kW and 48 V was selected to drive the vehicle. Its torque constant Kt is 0.12 Nm/A, back-EMF constant Ke is 0.12 V/rad/s, and winding resistance is 0.05 Ω. The rated torque is 10 Nm, with a peak torque of 25 Nm and efficiency greater than 90% across 60–80% of its operating range. The selection of this motor is based on its ability to achieve the target top speed of ~60 km/h, accelerate a 670 kg vehicle with a payload up to 200 kg within 12–15 s, and maintain adequate efficiency for urban stop-and-go driving typical of three-wheelers. The torque-speed characteristics show sufficient performance margin for both loaded and unloaded conditions, while the compact size and air-cooling make it well suited for retrofitted three-wheel vehicles. The model accounts for electrical and mechanical dynamics, and its parameters are set based on manufacturer datasheets to reflect the tuktuk operations. Mechanical and electrical parameters of the motor are presented in Table 2 [20].

Table 2. Specifications of 3 kW BLDC motor [20].

Feature	Specification
Voltages	48/72/96 V
Rated power	3 kW
Peak power	6 kW
Current	50–70 A
Speed	3000–5000 rpm
Rated torque	10 Nm
Peak torque	25 Nm
Efficiency	>90%
Dimensions	18 cm diameter, 15 cm height
Weight	7.35 kg
Cooling	Air cooling

3.1.6. Vehicle body

The vehicle body consists of fundamental mechanical components, such as the tyres, chassis, differential, and gearbox. These parts work together to transmit the motor's power to the wheels, enabling vehicle movement. During this process, several forces like rolling resistance, aerodynamic drag, and road slope are taken into account. The effectiveness of the power transfer and overall vehicle performance is analyzed by comparing the actual output with the input drive cycle, providing insights into the vehicle's efficiency and dynamic behavior. Table 3 presents the vehicle body parameters as described.

Table 3. Presents the vehicle body parameters.

Parameter	Value	Unit
Vehicle mass	670	kg
Frontal area	2.91	m^2
Drag coefficient	0.15	--
Air density	1.225	kg/m^3
Gravitational acceleration	9.81	m/s^2

The complete simulation model consists of several components, including the vehicle body, controller, motor, battery pack, power converter, and drive cycle source, as illustrated in Figure 3. See Appendix A (A0–A8) for the full mathematical model.

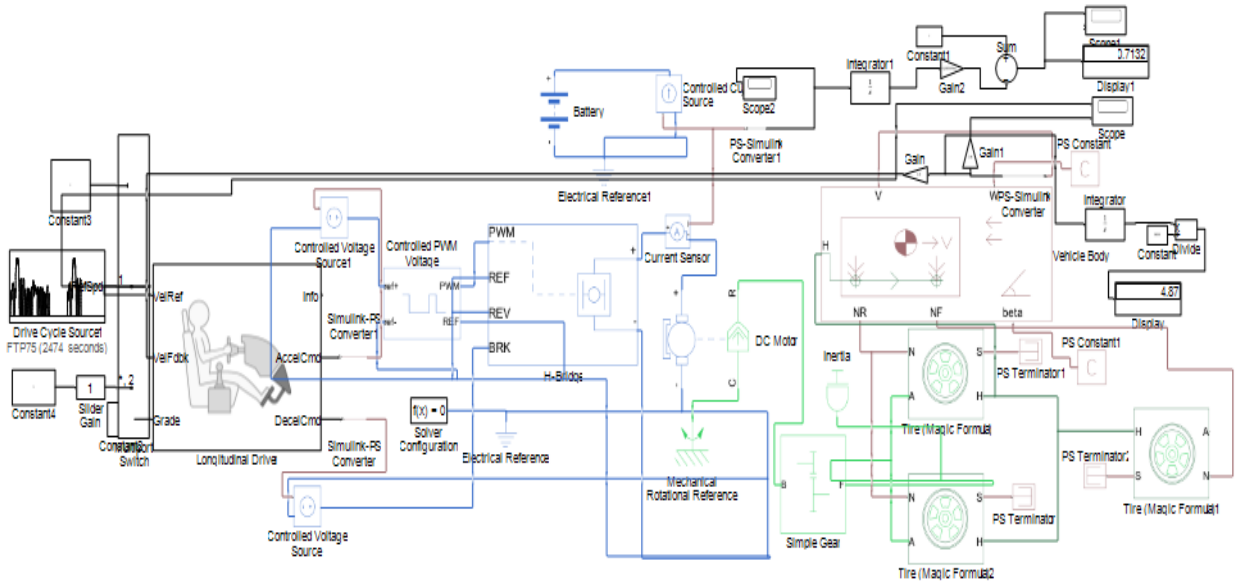

Figure 3. Complete MATLAB Simulink model of an electric three-wheel vehicle.

4. Results and discussion

4.1. Analysis of simulation results and efficiency comparison

Results of the four drive cycles deployed in the simulation are presented here. Input and output results of the simulations, which are run for various driving cycles, are shown in Table 4.

Table 4. The simulation input parameters for various drive cycles.

Drive cycle	FTP-75	NEDC	WLTP Class 3	UDDS
Simulation time (s)	2474	1180	1800	1369
Vehicle body weight (kg)	670	670	670	670
Frontal area (m^2)	2.91	2.91	2.91	2.91
Drag coefficient	0.15	0.15	0.15	0.15
Rolling resistance force (N)	0.015	0.015	0.015	0.015
Battery nominal voltage (V)	300	300	300	300
DC motor rated load (kW)	3	3	3	3
DC supply voltage (V)	48	48	48	48
H-bridge output voltage amplitude (V)	300	300	300	300

A. FTP-75 drive cycle

Characteristics of FTP75 drive cycle with respect to speed, current, and state of charge are shown in Figure 4 (a, b, and c), respectively.

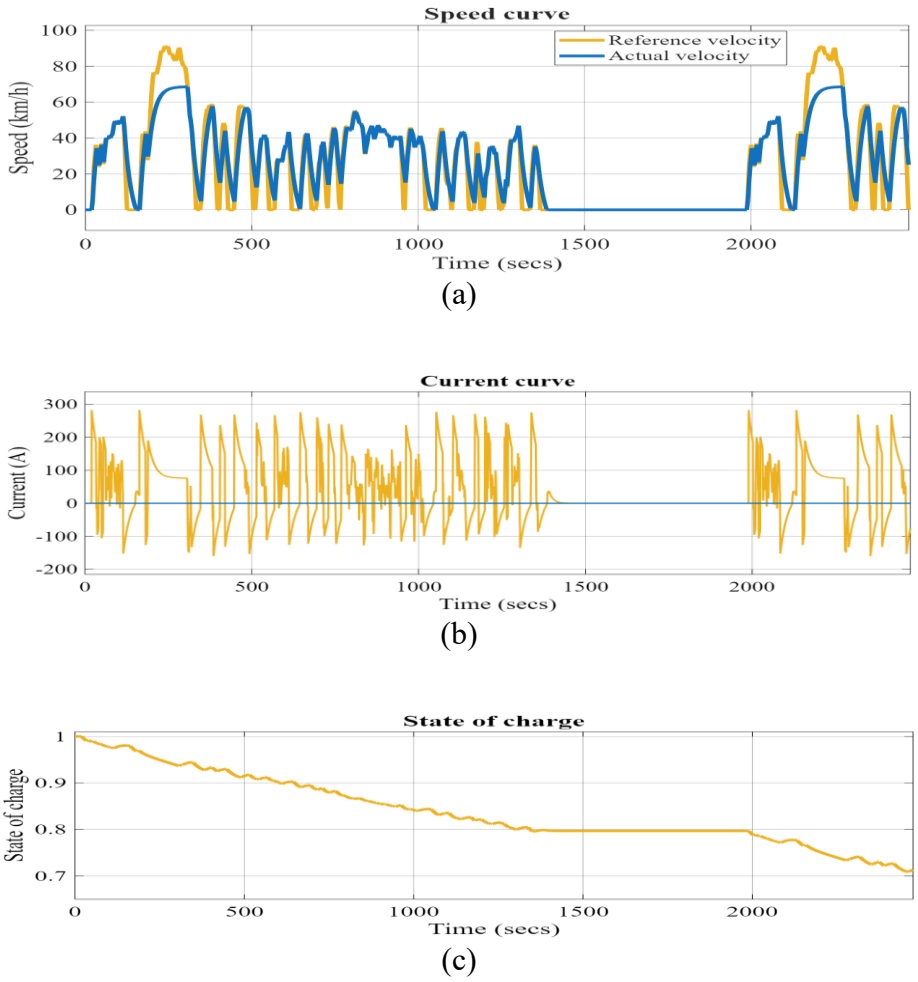

Figure 4. FTP-75 drive cycle characteristics.

Figure 4a shows the vehicle's reference velocity and actual velocity almost match, with the reference maximum cycle speed is 91.25 km/h, while the actual achieved speed was ~70 km/h due to motor and controller limitations. Figure 4b shows the variation in current during vehicle operation. As the speed increases, more current is drawn from the battery to meet the power demand. During regenerative braking, the current drops to negative values, indicating that energy is being fed back into the battery for charging. Figure 4c display the battery's SOC for 2474 s, ranging from 100% to 71%. Also, 29% of the battery is consumed for 4.87 km at 2474 s. The SOC curve rises at certain points due to regenerative braking.

B. NEDC drive cycle

Characteristics of NEDC drive cycle with respect to speed, current, and state of charge are shown in Figure 5 (a, b, and c), respectively.

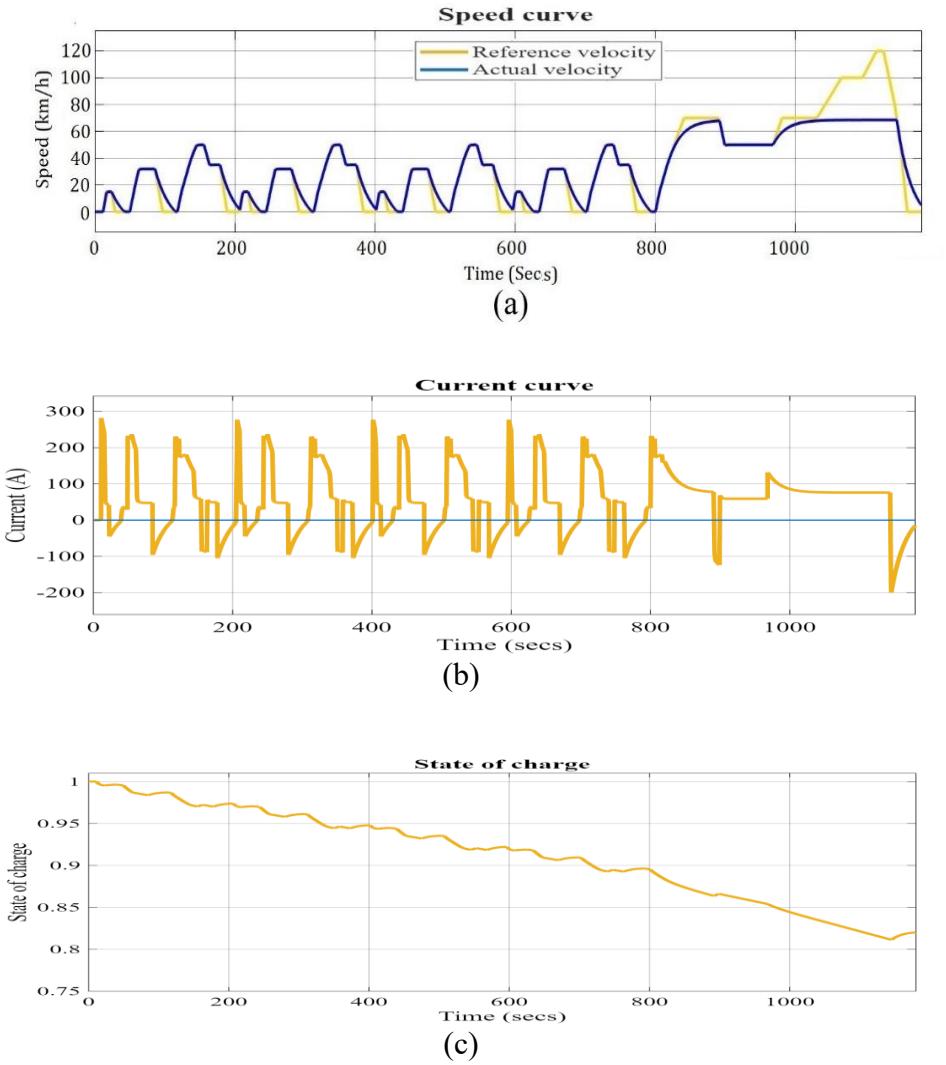

Figure 5. NEDC drive cycle characteristics.

Figure 5a shows the vehicle's reference velocity and actual velocity almost match, with the reference maximum cycle speed above 100 km/h, while the actual achieved speed was ~70 km/h due to motor and controller limitations. Figure 5b shows the variation in current over time. As vehicle speed increases, more current is drawn from the battery to meet the rising power demand. During regenerative braking, the current curve dips into the negative region, indicating that energy is being fed back into the battery for charging. Figure 5c illustrates the battery's SOC over a simulation period of 1180 s. During this time, the SOC decreases from 100% to 81%, indicating that 19% of the battery is consumed for the vehicle to travel for around 2.94 km at 1180 s. The slight increases observed in the SOC curve at certain points are due to regenerative braking, which recovers energy and recharges the battery.

C. WLTP Class 3 drive cycle

Characteristics of WLTP Class 3 drive cycle with respect to speed, current, and state of charge are shown in Figure 6 (a, b, and c), respectively.

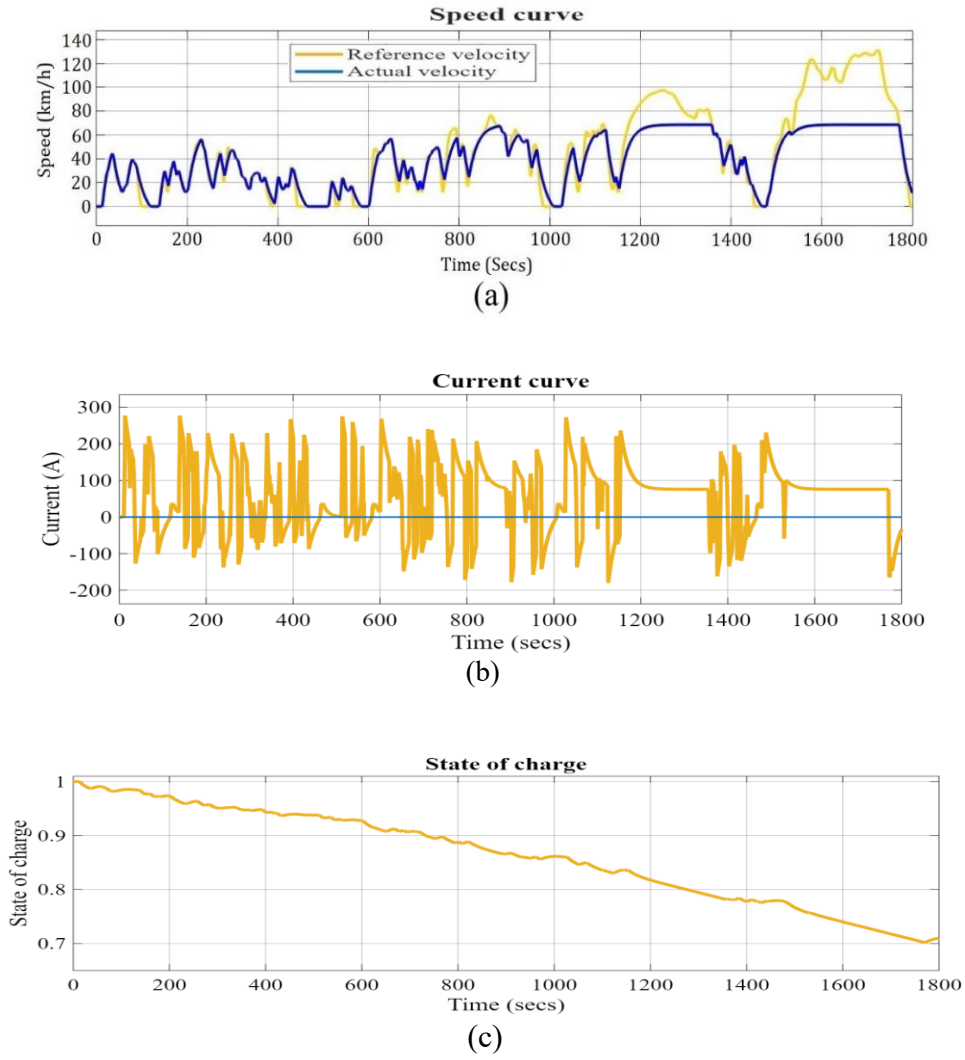

Figure 6. WLTP Class 3 drive cycle characteristics.

Figure 6a shows that the vehicle's reference velocity and actual velocity almost match, with the reference maximum cycle speed being 100 km/h, while the actual achieved speed was ~70 km/h due to motor and controller limitations. Figure 6b shows the variation in current over time. As vehicle speed increases, more current is drawn from the battery to meet the rising power demand. During regenerative braking, the current curve dips into the negative region, indicating that energy is being fed back into the battery for charging. Figure 6c shows the SOC of the battery over a simulation duration of 1800 s. During this period, the SOC decreases from 100% to 70%, indicating that 30% of the battery capacity is consumed as the vehicle travels 5.41 km in 1800 s. Occasional increases in the SOC curve are observed due to regenerative braking, which contributes to recharging the battery.

D. UDDS drive cycle

Characteristics of the UDDS drive cycle with respect to speed, current, and state of charge are shown in Figure 7 (a, b, and c), respectively.

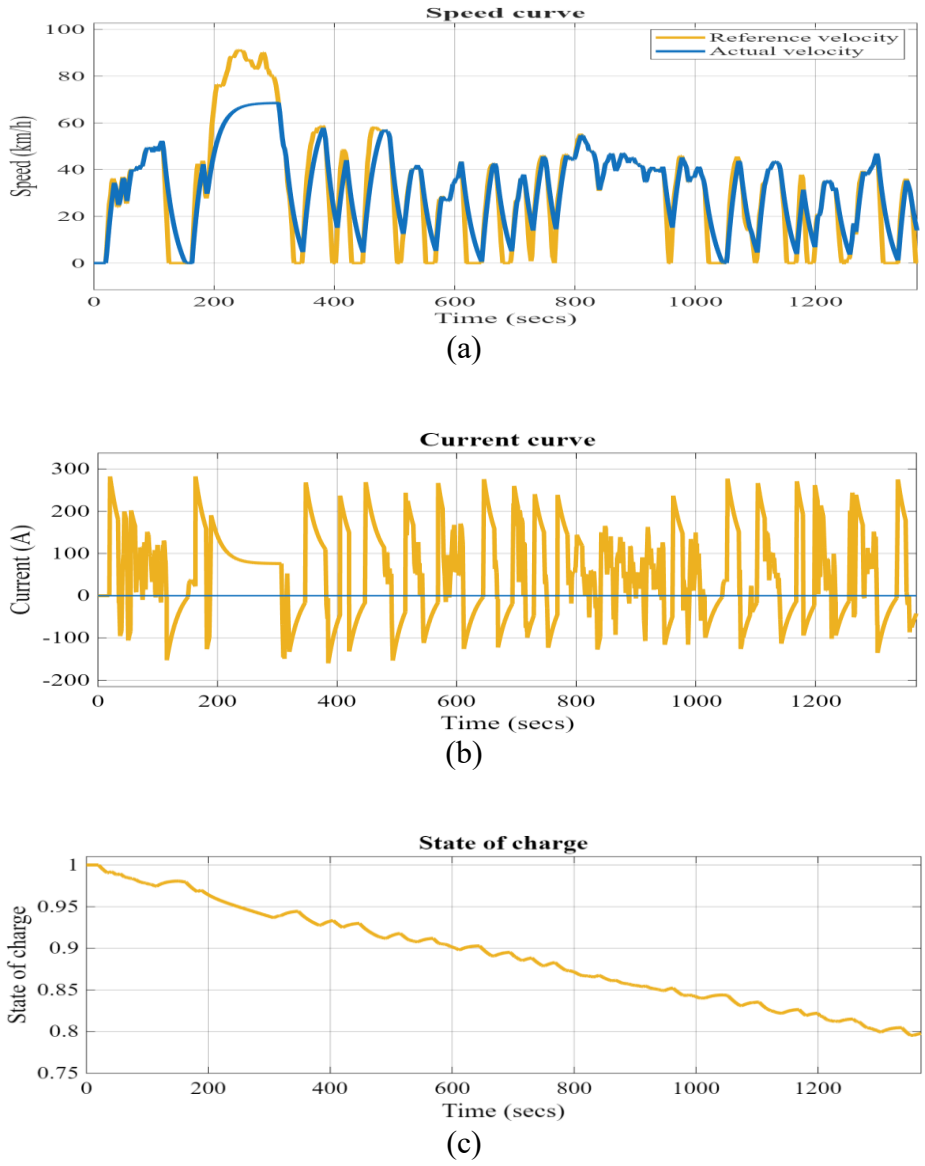

Figure 7. UDDS drive cycle characteristics.

Figure 7a shows that the vehicle's reference velocity and actual velocity almost match, with the reference maximum cycle speed being 91.25 km/h, while the actual achieved speed was ~70 km/h due to motor and controller limitations. Figure 7b shows the variation in current over time. As vehicle speed increases, more current is drawn from the battery to meet the rising power demand. During regenerative braking, the current curve dips into the negative region, indicating that energy is being fed back into the battery for charging. Figure 7c illustrates the battery's SOC over 1369 s, showing a decrease from 100% to 80%, meaning 20% of the battery is used to travel 3.38 km at 1369 s. Minor rises in the SOC curve are due to regenerative braking, which helps recharge the battery. Minor mismatches between the reference and actual speed above 60 km/h in the four-drive cycle are attributed to system torque limits and the PI controller dynamics.

The comparative analysis of the different drive cycles is illustrated in Table 5.

Table 5. The simulation output values of various drive cycles.

Name of drive cycle and simulation time (s)	SOC at the end of the drive cycle (Initial SOC was 100%)	Top speed (km/h)	Top speed reached?
FTP-75, 2474	71%	91.25	Yes
NEDC, 1180	81%	120	Yes
WLTP Class 3, 1800	70%	131.3	Yes
UDDS, 1369	80%	91.25	Yes

Each drive cycle serves a specific purpose and is designed to evaluate different aspects of vehicle performance, such as fuel economy, emissions, and driving behavior, under various conditions. The WLTP Class 3 drive cycle is more realistic and comprehensive. Other types of drive cycles, like the FTP75, NEDC, and UDDS, are less accurate for real-world driving, but they are simpler and have been widely used for consistency and regulation [13]. The choice of drive cycle depends on the specific goals of the test, such as assessing emissions, fuel economy, or vehicle performance in particular environments.

Comparing the simulations of EVs using different drive cycles, such as the FTP-75, NEDC, WLTP Class 3, and UDDS, provides a comprehensive understanding of how EVs perform under various real-world driving conditions. Each drive cycle is designed to simulate specific driving patterns, and the resulting performance metrics from these tests can reveal the strengths and limitations of EVs in terms of energy consumption, range, efficiency, and emissions. Table 6 illustrates the comparison of these four drive cycles.

Table 6. Key Parameters of the drive cycles FTP-75, NEDC, WLTP Class 3, and UDDS.

Parameters	Type of drive cycles			
	FTP-75	NEDC	WLTP Class 3	UDDS
Region	USA	Europe	Global	USA
Test duration	2474 s	1180 s	1800 s	1369 s
Distance travelled	17.77 km	11. 03 km	23.27 km	12.07
Average speed	34.2 km/h	34 km/h	46.5 km/h	31.5 km/h
Maximum speed	97 km/h	120 km/h	131.3 km/h	90 km/h
Driving conditions	Urban, stop-and-go traffic	Urban and highway, mixed	Mixed urban, rural, highway	Urban, stop-and-go traffic
Key characteristics	Mixed city/highway driving with frequent stops and accelerations	Combination of urban and extra-urban driving with steady speed	More dynamic, with higher speeds and aggressive acceleration	Urban driving with many stops and starts

The average speed for each drive is obtained by dividing the distance travelled over the period of simulation in hours. The WLTP Class 3 drive cycle is most appropriate for electric tuktuks because it offers a more accurate and realistic representation of their energy consumption, range, and performance under typical usage conditions. It allows manufacturers to optimise designs for urban driving, which is the primary domain for tuktuks, and provides consumers with reliable information to understand the vehicle's real-world performance.

4.2. Impact of WLTP Tuktukdrive cycle on electric tuktuk performance

The superiority of WLTP Class 3 is supported not only by SOC and energy consumption trends but also by its more realistic representation of mixed urban-suburban-highway driving conditions. Unlike FTP-75 and UDDS, which emphasize stop-and-go traffic, WLTP includes higher acceleration variability and broader speed ranges, better reflecting the operational patterns of urban three-wheelers. This connection between SOC trends (Table 7) and dynamic cycle characteristics provides a stronger justification for selecting WLTP Class 3 as the most representative.

The WLTP is a globally recognised and advanced drive cycle designed to simulate real-world driving behavior more accurately than other standards. For electric Tuktuktuktuks, which are typically used in urban and semi-urban environments, the WLTP drive cycle plays a critical role in assessing and enhancing vehicle performance. It impacts energy consumption, range estimation, thermal management, and battery life, while also providing insights for component durability, powertrain optimization, and regulatory compliance. The higher energy consumption observed in heavier vehicles is primarily attributed to increased rolling resistance and greater inertial demand during acceleration phases. As vehicle mass rises, the required tractive effort to overcome both inertia and drag forces increases proportionally, leading to higher motor current draw and deeper SOC depletion. Moreover, the regenerative braking efficiency slightly decreases with increased mass, as the braking torque becomes limited by inverter and motor constraints, reducing the fraction of recoverable energy. These physical interactions collectively explain the consistent upward trend in energy consumption with vehicle weight under WLTP conditions, as shown in Table 7. This implies that an increase in the mass of the electric tuktuk is directly proportional to energy consumption but inversely proportional to the instantaneous SOC.

EVs must select the appropriate driving profile based on a precise assessment of a number of unique key parameters, such as different driving ranges, energy consumption, battery life cycle, life expectancy, and overall system warranty problems. The WLTP stands out as a promising option, as it closely reflects the real-world driving patterns of EVs, especially electric cars, in the absence of a globally recognised standardized driving profile specifically designed for EVs. As it is essential for accurate and reliable performance assessments of EVs, adopting a comprehensive global standard for driving cycles is no longer optional but necessary, considering the rapid expansion of EVs in the automotive industry.

Based on the MATLAB Simulink simulation graphs for the WLTP Class 3 drive cycle, the impact of different masses on energy consumption is presented in Table 7.

Table 7. Vehicle mass and energy consumption of the WLTP class 3 drive cycle.

Vehicle mass (kg)	SOC at the end of the drive cycle (Initial SOC 100%)	Energy consumption after 1800 seconds in kWh
670	70.0	1.440
800	66.4	1.612
1000	60.7	1.886
1200	55.0	2.160
1400	49.3	2.434
1600	43.6	2.695
1800	37.9	2.986
2000	32.2	3.255

Energy consumed for each simulated vehicle mass is obtained using Eq (5).

$$Energy\ Consumed = \left(\frac{SOC_{initial} - SOC_{final}}{100}\right) \times Battery\ Total\ Energy \quad (5)$$

A sensitivity analysis was performed by varying vehicle mass from 670 kg to 2000 kg to evaluate the robustness of the simulation results. The monotonic increase in energy consumption observed across these scenarios, as shown in Table 7, confirms the physical consistency of the model, as higher mass directly increases rolling and inertial loads. The smooth and predictable trend in SOC reduction also indicates numerical stability and validates the reliability of the modelling framework for performance prediction across a range of operating conditions. The simulation results demonstrate that energy consumption increases significantly with vehicle mass. As the vehicle mass increases, energy consumption also rises. A lighter vehicle of 670 kg uses only 30% of the battery after 1800 s (30 minutes), while a heavier one of 2000 kg uses nearly 68%. Table 7 shows that when the weight of a vehicle increases, the battery tends to discharge faster. This happens for a few reasons:

Increased energy demand: A heavier vehicle requires more energy to move, especially when accelerating or climbing hills. This means that the motor needs more power to overcome the additional weight, leading to higher energy consumption.

More power to maintain speed: A heavier vehicle requires more energy to maintain a constant speed, as it has more inertia. The engine or motor works harder to keep it moving, causing the battery to drain faster.

Table 8. Comparative summary of this study and related works.

Aspect	Existing literature	This work
Vehicle type focus	[8]—Mostly four-wheel vehicles	Unlike many studies that generalise EV conversions for four-wheel passenger cars, this paper specifically targets three-wheel vehicles (like electric tuktuks), which are widely used in developing countries. This provides a more practical, application-specific contribution to sustainable urban mobility.
System coverage	[12,21,22]—Often limited to individual components	This work integrates all critical components (vehicle body, DC motor, H-bridge, PID controller, battery, and drive cycles) into a single, complete simulation framework using MATLAB Simulink. Many previous studies focus only on motor or battery performance without a fully coupled system model.
Drive cycles and real-world vehicle dynamics	[15,16,18,19,21,22]—Usually, one or two drive cycles	This paper uses four different standard drive cycles (FTP-75, NEDC, WLTP Class 3, UDDS), offering a more realistic and diverse performance evaluation. Many existing papers use only a single drive cycle, which limits the reliability and applicability of the results.
Battery capacity estimation and SOC tracking	[10–12,16,21,22]—Basic or sometimes missing	The paper detailed the analysis of battery voltage, current, power, and SOC variation. Some literature focuses mainly on vehicle dynamics or motor control, missing the critical aspect of energy consumption over time. Unlike many papers that do not discuss battery sizing in detail, this paper mentions the required battery capacity to meet specific performance and range targets.

Battery efficiency: In EVs, heavier weight increases strain on the battery, potentially reducing its overall efficiency. This also decreases the driving range, as the battery must supply more power to keep the vehicle moving. Six identified aspects from previous related works were noted and compared with the present study, and the details are provided in Table 8.

These findings have immediate real-world relevance. For example, operators of commercial three-wheelers can use WLTP-derived energy consumption rates to optimize route scheduling and charging intervals. Manufacturers can use mass-based SOC trends to refine chassis design, battery placement, and structural weight distribution. The strong dependency of energy usage on mass also highlights the importance of lightweight materials in future electric rickshaw development.

5. Conclusions

This study developed a detailed component-level MATLAB/Simulink framework for evaluating the dynamic performance and energy consumption of a three-wheel EV under standard driving conditions. The integration of a 3 kW BLDC motor, a 48 V 100 Ah lithium-ion battery, and an H-bridge inverter enabled realistic modelling of current demand, torque response, and state-of-charge variation across four widely used drive cycles: FTP-75, UDDS, NEDC, and WLTP Class 3.

A comparative analysis of the cycles revealed that WLTP Class 3 is the most suitable and representative drive cycle for three-wheel EVs operating in developing-country urban traffic. This is because WLTP Class 3 incorporates a broader range of speed variations, longer acceleration periods, and mixed low-to-medium-speed segments that closely mirror the real-world duty patterns of commercial three-wheelers (tuktuks). In contrast, FTP-75 and UDDS mainly capture low-speed stop-and-go behavior typical of dense inner-city movement, while NEDC represents smoother and less dynamic peri-urban travel. These cycles remain useful for benchmarking, but WLTP Class 3 provides a more realistic basis for evaluating motor sizing, controller tuning, and energy-efficiency performance.

In practical terms, this study provides a technical basis for selecting suitable drive cycles for design validation, optimizing energy consumption for urban fleet operators, and informing retrofit guidelines for transitioning ICE three-wheelers to electric platforms. WLTP Class 3 emerges as the preferred benchmark for manufacturers due to its balanced representation of real-world speed transients. Mass-based simulation trends offer actionable insights into payload limits, energy planning, and chassis design improvements. Future work will incorporate experimental validation and advanced control strategies to support industrial deployment.

Use of AI tools declaration

The authors declare they have not used Artificial Intelligence (AI) in the creation of this article.

Acknowledgements

This research was funded by the National Research Foundation, South Africa, with grant reference SRUG2205025715.

Conflict of interest

The authors declare no conflicts of interest.

Author contributions

M M Mostafa Almadani: Conceptualization, Methodology, Software, Formal analysis, Writing—original draft preparation. Omowunmi Mary Longe: Supervision—review and editing. Lanre Olatomiwa: Supervision—review and editing. Tobiloba Somefun: Methodology, Formal analysis, Writing—review and editing.

References

1. Keegan G, Nelendran P, Oluwafemi O (2024) Modeling and simulation of hybrid electric vehicles for sustainable transportation: Insights into fuel savings and emissions reduction. *Energies* 17: 5225. https://doi.org/10.3390/en17205225
2. Nascimento L, Kuramochi T, Woollands S, et al. (2022) Greenhouse gas mitigation scenarios for major emitting countries: Analysis of current climate policies and mitigation commitments: 2022 update. Report. Available from: https://newclimate.org/sites/default/files/2022-10/EC-PBL2022_CurrentPolicies_Oct22.pdf.
3. Francis J, Narayamparambil AB, Johnson A, et al. (2021) Conversion of internal combustion engine car to semi-autonomous electric car. *J Phys: Conf Ser* 2070: 012203. https://doi.org/10.1088/1742-6596/2070/1/012203
4. Almadani M, Oni OE, Longe OM, et al. (2024) Comparison of battery chemistries for electric vehicle applications. *5th African International Conference on Industrial Engineering and Operations Management*. https://doi.org/10.46254/AF05.20240159
5. Sharmila B, Srinivasan K, Devasena D, et al. (2022) Modelling and performance analysis of electric vehicle. *Int J Ambient Energy* 43: 5034–5040. https://doi.org/10.1080/01430750.2021.1932587
6. Oni OE, Longe OM (2024) A study on electric vehicle footprint in South Africa. *Energies* 17:6086. https://doi.org/10.3390/en17236086
7. Dassault Systèmes (2024) SolidWorks, Version 2024. Dassault Systèmes, Waltham, MA. Available from: https://www.solidworks.com/support/downloads.
8. Hossain M, Hasan M, Hasanuzzaman M, et al. (2023) Affordable electric three-wheeler in Bangladesh: Prospects, challenges, and sustainable solutions. *Sustainability* 15: 149. https://doi.org/10.3390/su15010149
9. Vražić M, Vuljaj D, Pavasović A, et al. (2014) Study of a vehicle conversion from internal combustion engine to electric drive. *IEEE International Energy Conference (ENERGYCON)* 1544–1548. https://doi.org/10.1109/ENERGYCON.2014.6850628
10. Qiao Q, Zhao F, Liu Z, et al. (2019) Electric vehicle recycling in China: Economic and environmental benefits. *Resour, Conserv Recycl* 140: 45–53. https://doi.org/10.1016/j.resconrec.2018.09.003

11. Gautam AK, Tariq M, Pandey JP, et al. (2022) Optimal power management strategy by using fuzzy logic controller for BLDC motor-driven e-rickshaw. *J Intell Fuzzy Syst* 42: 1089–1098. https://doi.org/10.3233/JIFS-189774
12. Suryavanshi SS, Ghanegaonkar PM, Kawade RK (2025) Insights into retrofitting internal combustion engine vehicles to battery electric vehicles for eco-friendly vehicle technology. *SAE Mobilus*. https://doi.org/10.4271/2025-01-5009
13. Kulkarni AR, Singh S, Kant K, et al. (2024) Experimental electric retrofitting of an ICE vehicle with simulation and cost analysis. *Int J Innovative Technol Explor Eng* 9: 45–50. https://doi.org/10.35940/ijitee.I1008.0799S20
14. Pandit H, Prajapati S, Kumar A, et al. (2024) Effective EV battery charging system using MPPT controller for solar PV system. *International BIT Conference (BITCON)*, 1–6. https://doi.org/10.1109/BITCON63716.2024.10984707
15. Gebisa A, Gebresenbet G, Gopal R, et al. (2021) Driving cycles for estimating vehicle emission levels and energy consumption. *Future Transp* 1: 615–638. https://doi.org/10.3390/futuretransp1030033
16. Tiwary A, Garg S, Mishra S (2022) Impact of driving behaviour on energy consumption of electric vehicle. *National Power Systems Conference (NPSC)*, 872–877. https://doi.org/10.1109/NPSC57038.2022.10069293
17. Pielecha J, Skobiej K, Kurtyka J (2020) Exhaust emissions and energy consumption analysis of conventional, hybrid, and electric vehicles in real driving cycles. *Energies* 13: 6423. https://doi.org/10.3390/en13236423
18. Yang JD, Millichamp J, Suter T, et al. (2023) A review of drive cycles for electrochemical propulsion. *Energies* 16: 6552. https://doi.org/10.3390/en16186552
19. Liu X, Zhao F, Hao H, et al. (2020) From NEDC to WLTP: Effect on the energy consumption, NEV credits, and subsidies policies of PHEV in the Chinese market. *Sustainability* 12: 5747. https://doi.org/10.3390/su12145747
20. Lakshmikanth S, Devarajaiah RM, Chowdhury A, et al. (2023) Analytical design of 3 kW BLDC motor for electric vehicle applications. *International Conference on Intelligent Technologies (CONIT)*, 1–7. https://doi.org/10.1109/CONIT59222.2023.10205842
21. Sabarish V, Dhayalan CD, Sriraman M, et al. (2023) Modeling and simulation of H-bridge motor-driven electric vehicle using MATLAB/Simulink. *International Conference on Artificial Intelligence and Smart Energy (ICAIS)*, 206–212. https://doi.org/10.1109/ICAIS56108.2023.10073813
22. Kokare B, Deokar S, Kale M (2025) Design and simulation of electric vehicle powertrain kinematics and components using MATLAB/Simulink. *Int Res J Adv Eng Manage* 3: 1587–1598. https://doi.org/10.47392/IRJAEM.2025.0257

Appendix A—Mathematical model used in simulink

A0. Notation & Typical parameter values

V_{bat}	Battery terminal voltage (V)
I_{bat}	Battery current (A), positive when discharging
SOC	State of charge (0–1)

C_{nom}	Battery nominal capacity (Ah)
R_{int}	Battery internal resistance (Ω)
$V_{oc}(SOC)$	Battery open-circuit voltage (V), function of SOC
P_{elec}	Electrical power drawn from battery (W)
V_{dc}	DC bus voltage
T_e	Electromagnetic torque produced by motor (N·m)
K_t	Motor torque constant (N·m/A)
K_e	Back-EMF constant (V·s/rad)
R_s	Stator (phase) resistance (Ω)
L_d, L_q	d- and q-axis inductances (H)
Ω	Rotor electrical angular speed (rad/s)
J	Rotating inertia (kg·m²) of motor + drivetrain
B	Viscous damping coefficient (N·m·s)
i_d, i_q	Motor d- and q-axis currents (A)
p	Number of pole pairs of motor
η_{mot}	Motor efficiency (fraction)
η_g	Gearbox/drivetrain efficiency (fraction)
r_w	Wheel radius (m)
g	Gravitational acceleration (= 9.81 m/s²)
m	Vehicle mass (kg)
A	Frontal area (m²)
C_d	Drag coefficient
ρ	Air density (kg/m³)
C_{rr}	Rolling resistance coefficient
V	Vehicle longitudinal speed (m/s)
F_{trac}	Traction force at wheel (N)
F_{res}	Total resistive forces (N)
D	PWM duty cycle
e_v	Speed tracking error (m/s)
K_p, K_i	PI controller gains

A1. Battery model (lumped, terminal model)

Open-circuit and terminal voltage:

$$V_{bat}(t) = V_{oc}\big(SOC(t)\big) - I_{bat}(t)\, R_{int}$$

where $V_{oc}(SOC)$ can be a lookup table (voltage vs SOC) or approximated linearly around the operating point.

SOC dynamics (Coulomb counting):

$$\frac{dSOC}{dt} = \frac{I_{bat}(t)}{3600\, C_{nom}}$$

(If SOC expressed 0–1, C_{nom} in Ah, and I_{bat} in A; sign convention positive when discharging.)

Electrical power from a battery:

$$P_{elec} = D(t)\, V_{dc}$$

(If regenerative: $I_{bat} < 0$, SOC increases)

A2. H-bridge/Inverter (average-model used for simulation)

Use an average (PWM) model mapping duty cycle D to phase voltage amplitude. For a two-level inverter with full-bridge:

Average DC-to-phase voltage (per phase, neutral-referenced):

$$V_{ph}(t) \approx D(t)\ V_{dc}$$

(When using space-vector or sinusoidal PWM, replace with the appropriate transform. For torque control, we usually map commanded current to duty via PWM law.)
DC bus current (approx):

$$I_{bat}(t) = \frac{P_{elec}(t)}{V_{bat}(t)}, \qquad P_{elec}(t) \approx \frac{T_e(t)\,\omega(t)}{\eta_{mot}\,\eta_g}$$

(Include inverter losses where desired.)

A3. BLDC motor dq-axis or simplified current-torque model

Two modelling options are common in Simulink: a full dq-model (more general) or a simplified current-torque model (sufficient for vehicle-level dynamics). Provide both; use whichever matches your model.

3.1. Simplified current-torque model (used if BLDC block maps i⟶T directly)

$$T_e(t) = K_t\, i_q(t)$$

$$\text{Back} - \text{EMF}\ \ e(t) = K_e\, \omega(t)$$

Electric equation (lumped)

$$V_{phase}(t) = R_s\, i(t) + L_s \frac{di(t)}{dt} + e(t)$$

But if you use a single-current model:

$$V_{phase,avg}(t) = R_s\, i(t) + L_s \frac{di(t)}{dt} + K_e\, \omega(t)$$

3.2. Full dq model (if you model field orientation/FOC)

$$v_d = R_s i_d + L_d \frac{di_d}{dt} - \omega L_q i_q$$

$$v_q = R_s i_d + L_d \frac{di_q}{dt} + \omega L_d i_d + \omega \psi_f$$

Electromagnetic torque:

$$T_e = \frac{3}{2} p (\psi_f i_q + (L_d - L_q) i_d i_q)$$

For surface-mounted BLDC where $(L_d \approx L_q)$ and ψ_f dominates,

$$T_e \approx \frac{3}{2} p \psi_f i_q \Rightarrow T_e = K_t i_q$$

A4. Motor mechanical dynamics (rotational to wheel)

Motor rotational:

$$J \frac{d\omega}{dt} = T_e - T_{load} - B\omega$$

Load torque reflected to motor shaft:

$$T_{load} = \frac{F_{res} r_w}{\eta_g} \text{ (if gearox reduces speed)}$$

Wheel torque relation:

$$T_{wheel} = T_e \cdot N_g \cdot \eta_g$$

where N_g is gearbox ratio (motor torque $\times N_g \rightarrow wheel\ torque$). If using direct drive, $N_g = 1$.

A5. Longitudinal vehicle dynamics (translational)

Net force and acceleration:

$$m \frac{dv}{dt} = F_{trac} - F_{res}$$

Traction force at the wheels:

$$F_{trac} = \frac{T_{wheel}}{r_w}$$

Resistive forces:

$$F_{res} = F_{rr} + F_{aero} + F_{grade}$$

where

$$F_{rr} = C_{rr} mg$$

$$F_{aero} = \frac{1}{2}\,\rho\,A\,C_d\,v^2$$

$$F_{grade} = mg\sin(\theta) \approx mg\,\theta \text{ (θ in radians)}$$

Combine:

$$m\,\frac{dv}{dt} = \frac{T_e\,N_g\,\eta_g}{r_w} - C_{rr}\,mg - \frac{1}{2}\,\rho A C_d v^2 - mg\,sin\theta$$

A6. Regenerative braking (energy recovery)

When the demanded torque is negative (braking), the motor acts as a generator. Regenerated current into the battery:

$$I_{regen} = \frac{P_{regen}}{V_{bat}}, \quad P_{regen} = \eta_{inv}\,\eta_{mot}\,T_g\omega$$

where T_g is the generator torque magnitude and η_{inv} inverter efficiency capturing bidirectional losses. In practice, clamp regen current to battery charge rate limit.

Constraint: battery charge current limit $I_{bat,min}$ (negative allowed):

$$I_{bat}(t) \geq -I_{max,chg}$$

A7. Controller—PI speed controller and torque/current mapping

Speed tracking error:

$$e_v(t) = v_{ref}(t) - v(t)$$

PI controller output (torque command):

$$T_{cmd}(t) = K_p e_v(t) + K_i \int_0^t e_v(\tau)\,d\tau$$

Saturation and safety limits:

$$T_{cmd,min} \leq T_{cmd}(t) \leq T_{cmd,max}$$

Map torque command to q-axis current reference):

$$i_{q,ref}(t) = \frac{T_{cmd}(t)}{K_t}$$

If using the current controller inner-loop: regulate $i_q\ to\ i_{q,ref}$ via the current PI.

If using direct torque control without an inner loop, convert to inverter duty via torque-to-voltage mapping and PWM: $D = f(i_{q,ref})$ as implemented in Simulink.

A8. Power balance & efficiencies

Mechanical power at the shaft:

$$P_{mech} = T_e \omega$$

Electrical power drawn from battery (approx):

$$P_{elec} = \frac{P_{mech}}{\eta_{mot}\eta_g} + P_{losses}$$

Battery current from power:

$$I_{bat} = \frac{P_{elec}}{V_{bat}}$$

where P_{elec} includes iron, copper, inverter conduction and switching losses, gearbox losses. If unavailable, lump losses as a percentage of P_{mech}.